ADVANCED FUNCTIONAL MATERIALS
www.afm-journal.de

Enhanced Tri-Atom Ru-Based Catalyst for Hydrogen Evolution Reaction via Rapid Pyrolysis of Precursor

Xiaoyang Ren, Mengjiao Li, Kaiyue Wang, Ruihu Lu, Mengge Lu, Panpan Li, Yi Yao, Shao Jin, Ziyun Wang,* and Shubo Tian**

Atomically precise supported nanocluster catalysts (APSNCs), with well-defined metal active sites, unique geometrical and electronic structures and metal–metal bonds, demonstrate excellent catalytic performance. However, the synthesis of APSNCs with well-defined active centers and stable structures remains a huge challenge due to uncontrollable aggregation during synthesis and catalytic reactions. Herein, the Ru_3 nanocluster catalysts uniformly dispersed on oxidized carbon nanotubes (Ru_3/OCNT) is successfully synthesized by using a rapid pyrolysis of precursor strategy. The obtained Ru_3/OCNT exhibits excellent catalytic performance for alkaline hydrogen evolution reaction (HER). The catalyst achieves an overpotential of 19 mV at a current density of 10 mA cm^{-2} in 1 M KOH solution, outperforming commercial 20 wt.% Pt/C and 5 wt.% Ru/C. Moreover, the mass activity of Ru_3/OCNT is 23.47 and 11.83 times higher than that of commercial Pt/C and Ru/C. Density functional theory (DFT) calculations reveal that the metal–metal interaction and metal–support interaction in Ru_3/OCNT effectively modulate the electronic structure of Ru atoms, lower the hydrogen adsorption energy of the catalytic site, and promote the H* desorption. This work offers a new perspective on the design and synthesis of APSNCs with excellent alkaline hydrogen evolution performance.

1. Introduction

Atomically precise supported nanocluster catalysts (APSNCs) are composed of metal clusters with precise atomic numbers that are stabilized on supports.[1–8] The size of the metal cluster falls between that of the single-atom and nanoparticle, thereby possessing distinct and uniform metal active sites, which renders it highly promising for diverse applications in the field of catalysis.[9–11] The adjacent metal active sites and synergies in APSNCs can empower new catalytic reaction pathways, reduce the reaction energy barrier, enhance catalytic activity, and overcome the barrier of single-atom catalysts that lack sufficient sites to accommodate reactants and intermediates.[12–16] Furthermore, the study of APSNCs offers a potential opportunity to reveal the real active site in the catalytic reaction and elucidate the reaction mechanism.[7,17,18] However, achieving precise control of the atomic number of APSNCs and preventing their agglomerating during catalytic reactions are great challenges to be solved.[19]

Against the backdrop of an accelerated energy industry transformation, hydrogen energy has emerged as a new solution to address the energy crisis and establish a modern energy system, owing to its advantages of zero pollution, high calorific value, abundant resources, and versatile applications.[20,21] As one of the pivotal half-reactions in water electrolysis, the hydrogen evolution reaction (HER) at the cathode has become an important research direction for the preparation of green hydrogen.[22,23] However, the kinetic reaction steps of alkaline HER are relatively complex and involve the adsorption and dissociation of intermediate.[24–29] Currently, noble metal catalysts are often used to reduce the overpotential of hydrogen evolution reactions, but the cost of catalysts is high due to the scarcity of precious metals.[30–32] The synthesis of APSNCs is expected to provide a way to utilize precious metals more

X. Ren, K. Wang, M. Lu, P. Li, S. Jin, S. Tian
State Key Laboratory of Chemical Resource Engineering
College of Chemistry
Beijing University of Chemical Technology
Beijing 100029, P. R. China
E-mail: tianshubo@mail.buct.edu.cn

M. Li, R. Lu, Z. Wang
School of Chemical Sciences
University of Auckland
Auckland 1010, New Zealand
E-mail: ziyun.wang@auckland.ac.nz

Y. Yao
National Synchrotron Radiation Laboratory
University of Science and Technology of China
Hefei 230026, P. R. China
E-mail: yiyao@mail.ustc.edu.cn

The ORCID identification number(s) for the author(s) of this article can be found under https://doi.org/10.1002/adfm.202503678

DOI: 10.1002/adfm.202503678

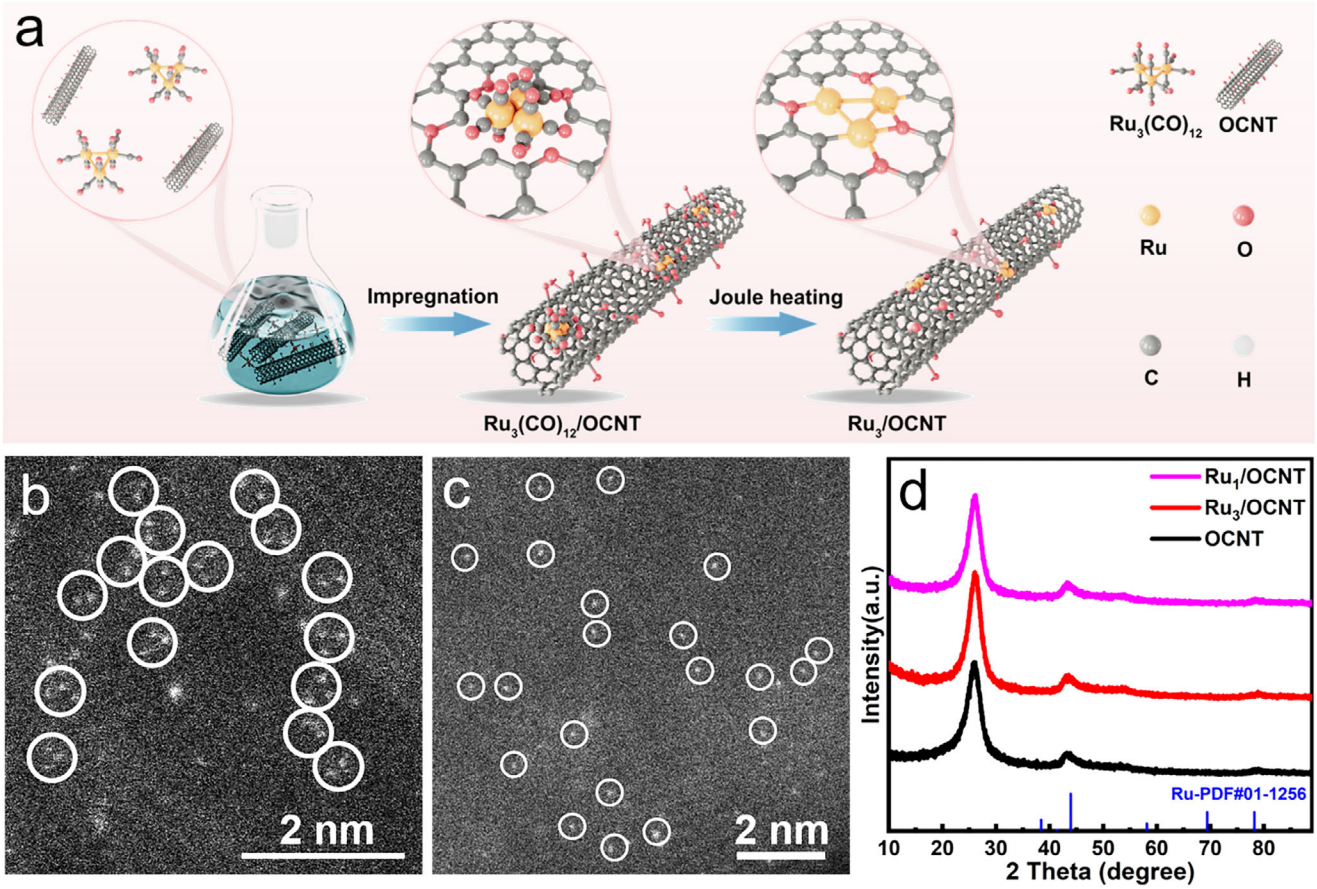

Figure 1. a) Schematic diagram of the synthesis of Ru_3/OCNT catalyst. b,c) AC HAADF-STEM images of Ru_3/OCNT and Ru_1/OCNT. d) XRD patterns for OCNT, Ru_3/OCNT, and Ru_1/OCNT catalysts.

economically and effectively. More importantly, an in-depth study of the relationship between the structure and properties of AP-SNCs could provide a promising framework for designing and optimizing catalysts at the atomic scale.

In recent years, Ru-based nanocatalysts have attracted increasing attention in the field of hydrogen production via water electrolysis due to their superior electrochemical activity. However, the strong adsorption hydrogen intermediates (H*) on Ru sites hinders the hydrogen desorption process, thereby limiting the electrocatalytic activity of the HER. Therefore, achieving Ru sites with optimal hydrogen desorption ability is crucial for enhancing HER performance.[33] Carbon materials are regarded as ideal supports owing to their exceptional electrical conductivity and high specific surface area.[34] Nevertheless, pure carbon supports can only form weak metal–support interactions with the active sites loaded on them, which is insufficient for effectively modulating the electronic structure of these active sites.[35] In contrast, the incorporation of O atoms into the carbon nanotube (OCNT) support enables the formation of robust interactions with metal active sites, such as Ru clusters.[36] The OCNT can not only enhance the stability of the Ru clusters but also facilitate electrons transfer from Ru to the support, thereby fine-tuning the electronic structure of Ru.

Herein, we reported a rapid pyrolysis of precursor strategy and successfully synthesized a tri-atom Ru-supported catalyst with outstanding catalytic performance for the alkaline hydrogen evolution reaction. The obtained Ru_3/OCNT catalyst, featuring precise atomic numbers, exhibited superior HER performance and stability exceeding that of commercial Pt/C and Ru/C under alkaline condition, achieving an overpotential of 19 mV at a current density of 10 mA cm^{-2}. DFT calculations demonstrated that the metal–metal interaction and metal–support interaction in Ru_3/OCNT modulated the electronic structure of Ru atoms, thereby reducing the hydrogen adsorption energy at the catalytic site, promoting the H* desorption, and accelerating HER kinetics.

2. Results and Discussion

The synthesis process of the Ru_3/OCNT catalyst is depicted in **Figure 1a**, wherein the OCNT utilized was obtained through acidification treatment. First, the precursor $Ru_3(CO)_{12}$ was impregnated onto the OCNT support ($Ru_3(CO)_{12}$/OCNT) using the room temperature impregnation method. Subsequently, heat treatment was employed to remove the carbonyl ligand and obtain Ru_3 clusters loaded on OCNT.[37,38] To prevent metal

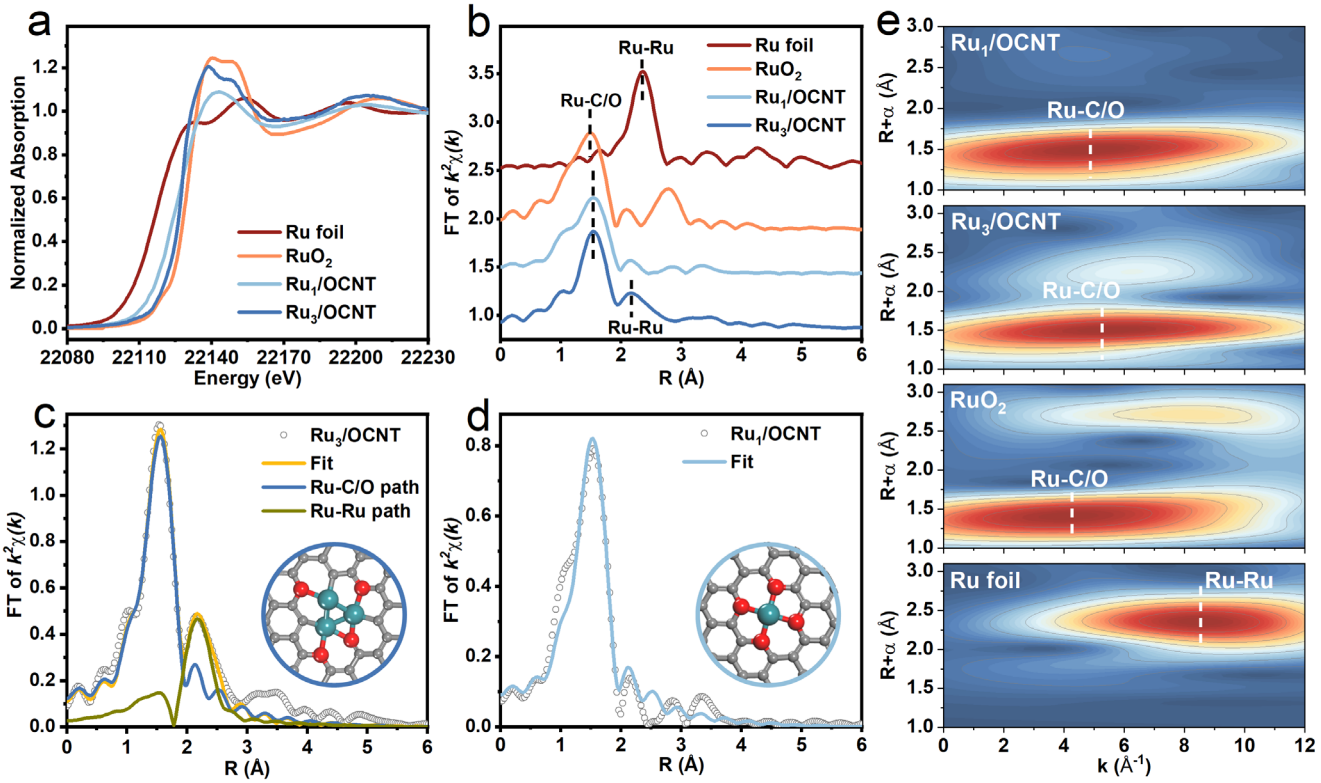

Figure 2. a) Normalized Ru K-edge XANES spectra for Ru_3/OCNT, Ru_1/OCNT, RuO_2 and Ru foil. b) k^2-weighted Fourier-transform Ru K-edge spectra for Ru_3/OCNT, Ru_1/OCNT, RuO_2 and Ru foil. EXAFS fitting curves for c) Ru_3/OCNT and d) Ru_1/OCNT at R space. Inset: the schematic model of Ru_3/OCNT and Ru_1/OCNT. C: grey, O: red, and Ru: Green. e) WT of the Ru K-edge EXAFS spectra for Ru_3/OCNT, Ru_1/OCNT, RuO_2 and Ru foil.

aggregation caused by prolonged exposure to high temperatures during heating, a fast Joule heating device was used, for rapid heating of $Ru_3(CO)_{12}$/OCNT located on the carbon cloth to 400 °C within 1–2 s and maintained at this temperature for 120 s before rapidly cooling down to room temperature.[6,39–41] Consequently, efficient removal of CO ligands could be achieved while enhancing the stability of Ru_3 nanoclusters on OCNT via Ru—C/O bonds. The resulting catalyst was designated as Ru_3/OCNT. In addition, a contrast catalyst named Ru_1/OCNT was synthesized using the same aforementioned strategy but with the replacement of the precursor by $RuCl_3 \cdot 3H_2O$ (see details in the Supporting Information).

The morphology and nanostructures of the Ru_3/OCNT catalyst were investigated using transmission electron microscopy (TEM) and high-resolution transmission electron microscopy (HRTEM). As shown in Figures S1–S3 (Supporting Information), in the electron microscopy images of Ru_3/OCNT, no discernible black spots attributed to Ru nanoparticles were observed on the multi-walled carbon nanotubes. Moreover, X-ray diffraction (XRD) analysis was performed to characterize the crystal structures of Ru_3/OCNT, Ru_1/OCNT, and OCNT. In addition to detecting the typical carbon diffraction peak, no characteristic diffraction peak corresponding to Ru was observed in the XRD patterns of both Ru_3/OCNT and Ru_1/OCNT (Figure 1d). Combining TEM and HRTEM images with XRD, it was determined that no aggregation occurred during both impregnation and pyrolysis, indicating highly dispersed Ru species. The loading of Ru in Ru_1/OCNT and Ru_3/OCNT were quantified by inductively coupled plasma-optical emission spectroscopy (ICP-OES), which were 0.13 and 1.285 wt.%, respectively. Atomic structure information was further obtained by aberration-corrected high-angle annular dark field scanning transmission electron microscope (AC HAADF-STEM). As shown in Figure 1b, Ru species could be clearly distinguished from carbon-based carriers according to the brightness difference-in the spherical aberration image of Ru_3/OCNT. It could be seen that Ru nanoclusters composed of three Ru atoms were the main metal species. A few single bright spots with uniform dispersion could be clearly seen in Figure 1c, demonstrating that Ru in the contrast catalyst Ru_1/OCNT was uniformly distributed on the OCNT substrate in the form of a single atom.

The valence state and local coordination environment of Ru in each catalyst were further probed using X-ray absorption spectroscopy. As shown in **Figure 2a**, the normalized X-ray absorption near edge structure (XANES) spectra of Ru K-edge revealed that the white line peak intensities of both Ru-based catalysts were located between the absorption edges of RuO_2 and Ru foil, indicating that the average valence of Ru species in the catalysts was between 0 and +4, with positive charge. This observation could be attributed to the charge transfer between Ru and OCNT. Subsequently, X-ray photoelectron spectroscopy (XPS) was employed to further investigate the elemental composition and surface electron states of the materials as well as determine the charge states of Ru in the two catalysts. As shown in Figure S5 (Supporting

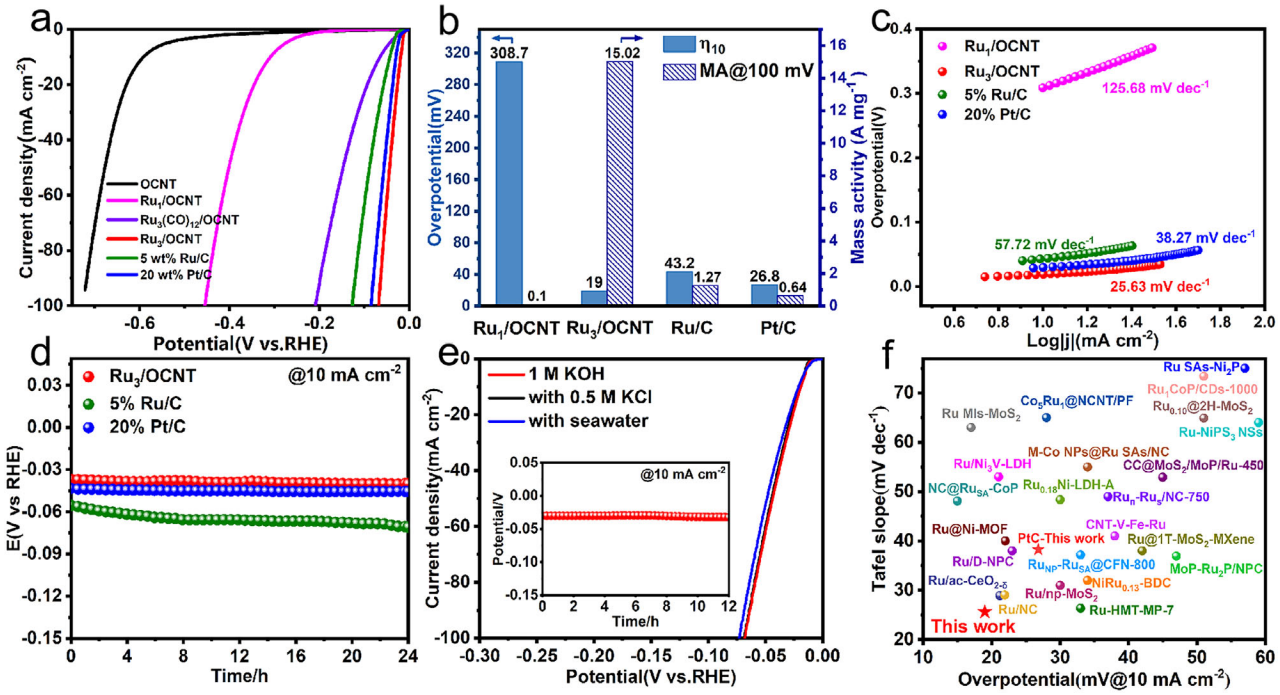

Figure 3. a) LSV curves for Ru_3/OCNT, Ru_1/OCNT, $Ru_3(CO)_{12}$/OCNT, OCNT, 5 wt.% Ru/C and 20 wt.% Pt/C measured in 1 M KOH. b) Comparisons of mass activity and c) Tafel curves for the Ru_3/OCNT, Ru_1/OCNT, 5 wt.% Ru/C and 20 wt.% Pt/C catalysts measured in 1 M KOH. d) Stability test for Ru_3/OCNT, 5 wt.% Ru/C and 20 wt.% Pt/C in 1 M KOH. e) LSV curves for Ru_3/OCNT measured in 1 M KOH with 0.5 M KCl and 1 M KOH with seawater. Inset: the stability test for Ru_3/OCNT measured in 1 M KOH solution with 0.5 M KCl. f) Comparison of the HER performance for Ru-based catalysts reported in the literature.

Information), The XPS survey spectrum of Ru_3/OCNT catalyst showed that the catalyst mainly contains C, O, and Ru elements, which was consistent with the EDS elemental mapping (Figure S4, Supporting Information). The fitted C 1s peak included the typical C—C, C—O, and C═O bonds. In the O 1s spectrum, in addition to the peaks of C—O and C═O, the characteristic peak of Ru—O located at 531.08 eV was also detected. Additionally, in high-resolution the Ru 3p XPS spectra (Figure S6, Supporting Information), the peaks at 464.07 and 486.47 eV corresponded to the binding energies of Ru $3p_{3/2}$ and Ru $3p_{1/2}$ respectively, indicating that the presence of Ru^{3+} species[42,43] was resulting from strong interactions between Ru_3 clusters and carbon oxide nanotubes[44] after ligand removal. Unfortunately, no effective Ru 3p signal was detected in the Ru_1/OCNT catalyst due to the low Ru loading in the catalyst.

The Fourier transform k^3-weighted extended X-ray absorption fine structure (FT-EXAFS) spectra of Ru_3/OCNT exhibited distinct peaks at ≈1.5 Å in R-space, indicating the presence of Ru-C/O scattering, and smaller peaks at ≈2.3 Å (Figure 2b), which could be attributed to Ru–Ru scattering,[45,46] respectively. The corresponding wavelet transformation (WT) contour plots provided visual representations of the local structure of Ru species in both the R and k spaces (Figure 2e). By comparing with reference WT plots obtained from Ru foil and RuO_2, it was observed that the WT image of Ru_3/OCNT displayed a prominent signal at ≈4.2 $Å^{-1}$ corresponding to the Ru—C/O scattering path, along with a weak WT signal at ≈8 $Å^{-1}$ associated with the Ru–Ru scattering path.[47,48] Conversely, only the presence of the Ru—C/O path at ≈4.2 $Å^{-1}$ was evident in the wavelet image obtained for the Ru_1/OCNT. To obtain quantitative structural parameters of Ru atoms, EXAFS curve fitting analysis was performed (Figure 2c,d), and detailed coordination information of all samples were summarized in Table S1 (Supporting Information). The fitting result for Ru_3/OCNT revealed an average coordination number (CN) of Ru—C/O and Ru–Ru was 2.5 and 1.8, respectively. On the contrast, in the Ru_1/OCNT catalyst, no coordination information belong to Ru–Ru path was observed, which verified that Ru was anchored on OCNT in the form of single atoms, with an average CN of 3.9 for the Ru—C/O coordination path.

Then, the HER performance of Ru_3/OCNT and the catalysts as contrast samples in 1 M KOH electrolyte at room temperature were evaluated using a standard three-electrode system. **Figure 3a** illustrated the LSV polarization curves of all catalysts. Proverbially, HER initial potential reflected the intrinsic activity of the catalyst and the onset potentials of Ru_3/OCNT, 5 wt.% Ru/C and 20 wt.% Pt/C were all close to zero, confirming that the three catalysts had excellent HER activity. At a current density of 10 mA cm^{-2}, Ru_3/OCNT demonstrated an overpotential of only 19.0 mV, surpassing Pt/C (26.8 mV), Ru/C (43.2 mV), and Ru_1/OCNT (308.7 mV). Moreover, the $Ru_3(CO)_{12}$/OCNT catalyst (without ligand removal) exhibited lower HER activity compared to Ru_3/OCNT. This could be attributed to the surface ligands on $Ru_3(CO)_{12}$/OCNT, which blocked certain metal active sites, consequently diminishing catalytic performance.[49] Furthermore, the removal of ligands allowed Ru atoms to form stronger interactions with the support matrix, thus -facilitating the optimization of both geometric and electronic configurations, which were

critical factors for enhancing electrocatalytic efficiency.[6,35] To address any concerns regarding different mass of supported Ru on the catalysts, we also compared the normalized mass activity of various catalysts under 100 mV (Figure 3b) and found that the mass activity of Ru_3/OCNT was 15.02 A mg^{-1}, which was 11.83 times that of Ru/C and 150.2 times that of Ru_1/OCNT. Moreover, we investigated the reaction kinetics by analyzing the Tafel curve (Figure 3c). Remarkably, compared with Pt/C (38.27 mV dec^{-1}), Ru/C (57.72 mV dec^{-1}), and Ru_1/OCNT (125.68 mV dec^{-1}) catalysts, Ru_3/OCNT displayed a significantly lower Tafel slope value at 25.63 mV dec^{-1}, indicating its superior reaction kinetics.[50]

In order to further investigate the internal activity relationship of the catalyst, cyclic voltammetry (CV) was employed to assess the double layer capacitance (C_{dl}) of the catalyst in the non-Faraday region at different scanning rates.[51,52] As shown in Figure S12 (Supporting Information), Ru_3/OCNT exhibited a significantly higher C_{dl} (136.57 mF cm^{-2}) compared to other catalysts, indicating a greater abundance of HER active sites on Ru_3/OCNT.[53] Subsequently, electrochemical impedance spectroscopy (EIS) was utilized to examine the electron transfer between the catalyst surface and the electrolyte.[54] As shown in Figure S13 (Supporting Information), Ru_1/OCNT displayed an enlarged Nyquist semicircle, suggesting an increased electron transfer resistance at interface. Conversely, Ru_3/OCNT exhibited the smallest nyquist semicircle, confirming efficient electron transport from its surface to the electrolyte.[55]

The common complexing agents, Ethylenediaminetetraacetic acid (EDTA) and potassium thiocyanate (KSCN), were employed to conduct toxicity tests on catalysts to ascertain whether the contribution to HER active site in Ru_3/OCNT catalyst was attributed to nanoclusters or single atoms. EDTA is mainly coordinated with Ru single atom, while KSCN can coordinate with all Ru species.[56–58] As shown in Figure S14 (Supporting Information), the HER current density on Ru_3/OCNT was only slightly decreased at 1 M KOH containing 10 mM EDTA compared to the original electrolyte. By contrast, after adding 10 mM KSCN to the electrolyte, the HER current density on Ru_3/OCNT dropped sharply, with raising η_{10} to 163.8 mV. Therefore, the significant activity gap in the electrocatalytic performance of Ru_3/OCNT poisoned by the two complexing agents clearly confirmed that Ru_3 clusters in Ru_3/OCNT were the main active sites for HER, rather than single atoms.

In addition, the stability parameter is a crucial criterion for evaluating the performance of the catalyst in catalytic reactions. Chronopotentiometry was used to evaluate the stability of Ru_3/OCNT in 1 M KOH. As shown in Figure 3d, the voltage of the Ru_3/OCNT catalyst exhibited negligible variation after 24 h electrolysis at the current density of 10 mA cm^{-2}, indicating that the catalyst had excellent stability. Long-term cyclic voltammetry was also commonly used to evaluate the stability of catalysts during the reaction. Figure S15 (Supporting Information) recorded the LSV polarization curve of Ru_3/OCNT after 1000 cycles, with no significant change compared with that before the cycle. The HRTEM image after 24 h stability test showed that Ru nanoclusters had no aggregation (Figure S16, Supporting Information). This was further verified by the absence of characteristic diffraction peaks of Ru in the XRD pattern, confirming the outstanding stability of Ru_3/OCNT against alkaline HER reaction. Furthermore, the Ru 3p XPS spectra (Figure S17c, Supporting Information) before and after the stability test were similar and the additional K peak in the C1s spectrum was attributed to the presence of residual electrolyte. The excellent stability of Ru_3/OCNT was attributed to the strong interaction between the nanoclusters and the OCNT support,[59] which protected the Ru_3 nanoclusters from aggregation. In addition, we evaluated the HER performance of Ru_3/OCNT under the conditions of alkaline seawater (1 M KOH + seawater) and alkaline simulated seawater (1 M KOH + 0.5 M KCl). In the simulated seawater, the LSV curves before and after the addition of KCl almost overlapped (Figure 3e). Moreover, at a current density of 10 mA cm^{-2}, the electrolytic voltage hardly changed within 12 h. Additionally, only a marginal performance decline was observed in alkaline seawater. The above results indicated that the Ru_3/OCNT catalyst had great application prospects in seawater electrolysis. Figure 3f compared the alkaline hydrogen evolution performance of Ru_3/OCNT with that of Ru-based catalyst reported in recent years, reflecting the excellent alkaline hydrogen evolution performance of Ru_3/OCNT.

In order to further elucidate the advantages of the atomic structure of Ru_3/OCNT, we performed first-principles calculations to investigate enhanced HER activity on Ru_3/OCNT (Ru-TAC) compared to Ru metal (Ru(0001)) and atomically dispersed Ru (Ru-SAC) at the atomic level. The coordination environments of SAC and TAC are composed of both C and O atoms, resulting in a variety of possible active site structures. Therefore, we calculated the formation energies of all possible structures, with detailed results shown in Figure S18 (Supporting Information). With the anchoring of carbon support, the Ru atoms can be atomically dispersed, while a strong metal-support interaction (SMSI) tailors the electronic structure of Ru atoms. As reported before,[60] traditional Ru-SAC does not demonstrate good HER activity. We found that Ru-TAC could offer a unique local environment of Ru atoms, likely due to the metal–support interaction and the interaction between metal-metal atoms. As a result, Ru-TAC exhibited superior HER activity, as indicated by our calculations. To further explore the mechanism, we built Ru-TAC, Ru-SAC, and Ru(0001) catalyst models (Figure S19, Supporting Information) and calculated the free energy change of HER process on the corresponding Ru atoms of these catalysts (Figure S20, Supporting Information). We observed that Ru(0001) showed a theoretical overpotential of 0.54 V in *H desorption step (**Figure 4a**), showing a strong H* adsorption while Ru-SAC also exhibited difficulty in *H desorption, leading to an overpotential of 0.46 V. Comparably, the Ru-TAC displayed a higher HER activity with a theoretical overpotential of 0.11 V, in agreement with our experimental findings.

Subsequently, charge density difference showed an interaction between Ru atoms and carbon/oxygen atoms and Ru atoms compared with Ru-SAC (Figure 4b). It suggested that metal interaction beyond SMSI was introduced to regulate the electronic structure. Several studies[61,62] have demonstrated that the deficiency in SMSI for tuning the electronic structure and the adsorption of intermediates, further leading to low activities to not become effective catalysts. In our system, Ru-TAC exhibited superior HER performance due to the co-effect of metal interaction and SMSI. These co-interactions not only improved the dispersion and stability of Ru but also optimized its electronic structure, thereby enhancing its catalytic activity. We further calculated the projector density of states (PDOS) of the Ru 4d orbitals

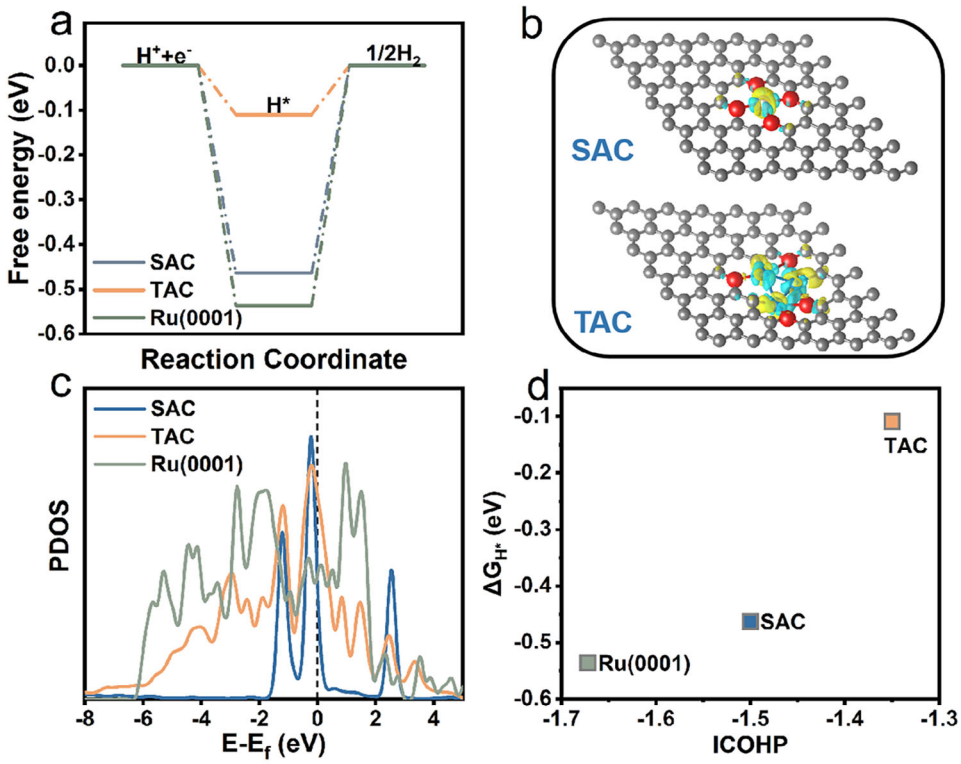

Figure 4. a) Free-energy diagram for the HER on SAC, TAC and Ru(0001) surface. b) The charge density between Ru and other atoms in SAC and TAC is shown, where yellow and blue colors denote electron accumulation and depletion, respectively. c) The d-orbital partial density of state (PDOS) plots of SAC, TAC and Ru(0001). d) Calculated integrated Crystal orbital Hamilton population (ICOHP) for the Ru—H bonds in different structures.

(Figure 4c). In general, a higher state at the Fermi level indicates that more active orbitals are interacting with adsorbed species. Accordingly, the highest state occurred on Ru(0001), followed by Ru-SAC, showing the stronger H* adsorption, agreeing with HER performance. The Ru-TAC exhibited the lowest density of states at the Fermi level, indicating weaker adsorption and, consequently, enhanced HER activity. This observation was further supported by the Crystal Orbital Hamilton Population (COHP) analysis (Figure S22, Supporting Information) and the integrated COHP (ICOHP) values calculated for the H—Ru bond. We found that as the ICOHP value increased, it suggested a decrease in H—Ru bonding (Figure 4d).

3. Conclusion

In summary, we synthesized Ru_3 nanocluster catalysts uniformly supported on carbon oxide nanotubes using the rapid pyrolysis of precursor strategy, and demonstrated that Ru_3/OCNT had excellent catalytic performance for alkaline HER, with a mass activity of 15.02 A·mg_{Ru}^{-1}, which was superior to commercial Pt/C and Ru/C. The structure of Ru_3/OCNT catalyst was characterized by AC HAADF-STEM and XAFS, and the results confirmed that the coordination number of Ru species with C/O and Ru were 2.5 and 1.8, respectively. DFT calculations showed that the high HER performance of Ru_3/OCNT was due to the most moderate hydrogen adsorption energy resulting from the metal interaction and the SMSI in the catalyst, which promoted the desorption of H*. This work provides a new idea for the design and synthesis of APSNCs with excellent alkaline hydrogen evolution properties.

Supporting Information

Supporting Information is available from the Wiley Online Library or from the author.

Acknowledgements

X.R., M.L., and K.W., contributed equally to this work. This work was financially supported by the National Key Research and Development Program of China (2021YFA1502200, 2023YFA1507400), the National Natural Science Foundation of China (22471012, 22101015). The authors thank the BL11B station in Shanghai Synchrotron Radiation Facility (SSRF). The computational study is supported by the Marsden Fund Council from Government funding (21-UOA-237) and Catalyst: Seeding General Grant (22-UOA-031-CGS), managed by Royal Society Te Apārangi. All DFT calculations were carried out on the New Zealand eScience Infrastructure (NeSI) high-performance computing facilities.

Conflict of Interest

The authors declare no conflicts of interest.

Data Availability Statement

Research data are not shared.

Keywords

atomically precise supported nanocluster, hydrogen evolution reaction, precursor strategy, rapid pyrolysis, strong metal–support interaction

Received: February 10, 2025
Revised: March 17, 2025
Published online:

[1] S. Mitchell, J. Pérez-Ramírez, *Nat. Rev. Mater.* **2021**, *6*, 969.
[2] Y.-M. Li, D. Shi, J. Yuan, R.-M. Zuo, H. Yang, J. Hu, S.-X. Hu, H. Sheng, M. Zhu, *Adv. Mater.* **2024**, *37*, 2412768.
[3] Y. Yun, H. Shen, Y. Shi, Y. Zhu, S. Wang, K. Li, B. Zhang, T. Yao, H. Sheng, H. Yu, M. Zhu, *Adv. Mater.* **2024**, *36*, 2409436.
[4] E. C. Tyo, S. Vajda, *Nat. Nanotech.* **2015**, *10*, 577.
[5] T. Imaoka, *Nat. Commun.* **2017**, *8*, 688.
[6] L. Yan, D. Wang, M. Li, R. Lu, M. Lu, P. Li, K. Wang, S. Jin, Z. Wang, S. Tian, *Angew. Chem., Int. Ed.* **2024**, *136*, 202410832.
[7] S. Ji, Y. Chen, Q. Fu, Y. Chen, J. Dong, W. Chen, Z. Li, Y. Wang, L. Gu, W. He, C. Chen, Q. Peng, Y. Huang, X. Duan, D. Wang, C. Draxl, Y. Li, *J. Am. Chem. Soc.* **2017**, *139*, 9795.
[8] C. Dong, Y. Li, D. Cheng, M. Zhang, J. Liu, Y.-G. Wang, D. Xiao, D. Ma, *ACS Catal.* **2020**, *10*, 11011.
[9] H. Wang, X. Liu, W. Yang, G. Mao, Z. Meng, Z. Wu, H.-L. Jiang, *J. Am. Chem. Soc.* **2022**, *144*, 22008.
[10] L. Yan, P. Li, Q. Zhu, A. Kumar, K. Sun, S. Tian, X. Sun, *Chem* **2023**, *9*, 280.
[11] L. Luo, R. Jin, *iScience* **2021**, *24*, 103206.
[12] Y. Si, Y. Jiao, M. Wang, S. Xiang, J. Diao, X. Chen, J. Chen, Y. Wang, D. Xiao, X. Wen, N. Wang, D. Ma, H. Liu, *Nat. Commun.* **2024**, *15*, 4887.
[13] M. Song, R. Zhang, B. Zhang, Z. Zhai, G. Liu, *Appl. Catal. B-Environ.* **2025**, *363*, 124787.
[14] L. Wang, J. Diao, M. Peng, Y. Chen, X. Cai, Y. Deng, F. Huang, X. Qin, D. Xiao, Z. Jiang, N. Wang, T. Sun, X. Wen, H. Liu, D. Ma, *ACS Catal.* **2021**, *11*, 11469.
[15] N. Wu, *Biosens. Bioelectron.* **2022**, *216*, 114609.
[16] S. Ji, Y. Chen, S. Zhao, W. Chen, L. Shi, Y. Wang, J. Dong, Z. Li, F. Li, C. Chen, Q. Peng, J. Li, D. Wang, Y. Li, *Angew. Chem., Int. Ed.* **2019**, *58*, 4271.
[17] T. Ding, X. Liu, Z. Tao, T. Liu, T. Chen, W. Zhang, X. Shen, D. Liu, S. Wang, B. Pang, D. Wu, L. Cao, L. Wang, T. Liu, Y. Li, H. Sheng, M. Zhu, T. Yao, *J. Am. Chem. Soc.* **2021**, *143*, 11317.
[18] W. Ye, S. Chen, Y. Lin, L. Yang, S. Chen, X. Zheng, Z. Qi, C. Wang, R. Long, M. Chen, J. Zhu, P. Gao, L. Song, J. Jiang, Y. Xiong, *Chem* **2019**, *5*, 2865.
[19] L. Li, Y.-F. Jiang, T. Zhang, H. Cai, Y. Zhou, B. Lin, X. Lin, Y. Zheng, L. Zheng, X. Wang, C.-Q. Xu, C. Au, L. Jiang, J. Li, *Chem* **2022**, *8*, 749.
[20] S. Chu, A. Majumdar, *Nature* **2012**, *488*, 294.
[21] J. Li, W. Yin, J. Pan, Y. Zhang, F. Wang, L. Wang, Q. Zhao, *Nano Res.* **2023**, *16*, 8638.
[22] Y. Jiang, Z. Liang, H. Fu, M. Sun, S. Wang, B. Huang, Y. Du, *J. Am. Chem. Soc.* **2024**, *146*, 9012.
[23] Q. Li, Z. Deng, D. Tao, J. Pan, W. Xu, Z. Zhang, H. Zhong, Y. Gao, Q. Shang, Y. Ni, X. Li, Y. Chen, Q. Zhang, *Adv. Funct. Mater.* **2024**, *34*, 2411283.
[24] S. Zhu, Z. Li, L. Hou, M. G. Kim, H. Jang, S. Liu, X. Liu, *Adv. Funct. Mater.* **2024**, *34*, 2314899.
[25] L. Zhang, H. Jang, Y. Wang, Z. Li, W. Zhang, M. G. Kim, D. Yang, S. Liu, X. Liu, J. Cho, *Adv. Sci.* **2021**, *8*, 2004516.
[26] Q. He, Y. Zhou, H. Shou, X. Wang, P. Zhang, W. Xu, S. Qiao, C. Wu, H. Liu, D. Liu, S. Chen, R. Long, Z. Qi, X. Wu, L. Song, *Adv. Mater.* **2022**, *34*, 2110604.
[27] Y. Jiao, Y. Zheng, *Angew. Chem., Int. Ed.* **2023**, *62*, 202307303.
[28] Z. Wang, K. Chi, S. Yang, J. Xiao, F. Xiao, X. Zhao, S. Wang, *Small* **2023**, *19*, 2301403.
[29] C. Yang, Z. Wu, Z. Zhao, Y. Gao, T. Ma, C. He, C. Wu, X. Liu, X. Luo, S. Li, C. Cheng, C. Zhao, *Small* **2023**, *19*, 2206949.
[30] J. M. Kim, J.-H. Kim, J. Kim, Y. Lim, Y. Kim, A. Alam, J. Lee, H. Ju, H. C. Ham, J. Y. Kim, *Adv. Mater.* **2020**, *32*, 2002210.
[31] Q. Li, Q. Zhang, W. Xu, R. Zhao, M. Jiang, Y. Gao, W. Zhong, K. Chen, Y. Chen, X. Li, N. Yang, *Adv. Energy Mater.* **2023**, *13*, 2203955.
[32] Y. Liu, Q. Wang, J. Zhang, J. Ding, Y. Cheng, T. Wang, J. Li, F. Hu, H. B. Yang, B. Liu, *Adv. Energy Mater.* **2022**, *12*, 2200928.
[33] W. Liu, Q. Chen, Y. Shang, F. Liu, R. He, J. Zhang, Q. Li, H. Chai, Y. Tan, S.-J. Bao, *Adv. Funct. Mater.* **2024**, *34*, 2410325.
[34] I. C. Gerber, P. Serp, *Chem. Rev.* **2020**, *120*, 1250.
[35] H. Wang, Y. Jiao, G. Zhang, W. Ma, W. Fan, X. Liu, Y. Zhao, H. Xie, W. Ma, X. Zong, *Adv. Funct. Mater.* **2024**, 2418617, https://doi.org/10.1002/adfm.202418617.
[36] R. Ding, L. Lin, C. Pei, X. Yu, Q. Sun, H. S. Park, *Chem. – A Eur. J.* **2021**, *27*, 11150.
[37] S. Tian, Q. Fu, W. Chen, Q. Feng, Z. Chen, J. Zhang, W.-C. Cheong, R. Yu, L. Gu, J. Dong, J. Luo, C. Chen, Q. Peng, C. Draxl, D. Wang, Y. Li, *Nat. Commun.* **2018**, *9*, 2353.
[38] H. Rong, S. Ji, J. Zhang, D. Wang, Y. Li, *Nat. Commun.* **2020**, *11*, 5884.
[39] M. Xie, Y. Lu, X. Xiao, D. Wu, B. Shao, H. Nian, C. Wu, W. Wang, J. Gu, S. Han, M. Gu, Q. Xu, *Adv. Funct. Mater.* **2024**, *35*, 2414537.
[40] B. Deng, R. A. Carter, Y. Cheng, Y. Liu, L. Eddy, K. M. Wyss, M. G. Ucak-Astarlioglu, D. X. Luong, X. Gao, K. JeBailey, C. Kittrell, S. Xu, D. Jana, M. A. Torres, J. Braam, J. M. Tour, *Nat. Commun.* **2023**, *14*, 6371.
[41] D. Xi, J. Li, J. Low, K. Mao, R. Long, J. Li, Z. Dai, T. Shao, Y. Zhong, Y. Li, Z. Li, X. J. Loh, L. Song, E. Ye, Y. Xiong, *Adv. Mater.* **2022**, *34*, 2104090.
[42] R. Ge, Y. Wang, Z. Li, M. Xu, S. Xu, H. Zhou, K. Ji, F. Chen, J. Zhou, H. Duan, *Angew. Chem., Int. Ed.* **2022**, *61*, 202200211.
[43] R. Ge, L. Li, J. Su, Y. Lin, Z. Tian, L. Chen, *Adv. Energy Mater.* **2019**, *9*, 1901313.
[44] Z. Wu, P. Yang, Q. Li, W. Xiao, Z. Li, G. Xu, F. Liu, B. Jia, T. Ma, S. Feng, L. Wang, *Angew. Chem., Int. Ed.* **2023**, *62*, 202300406.
[45] Q. Zhang, M. Lao, Y. Yu, X. Ma, M. Li, Z. Fei, P. J. Dyson, S. Wang, D. Min, *Adv. Funct. Mater.* **2024**, 2416071, https://doi.org/10.1002/adfm.202416071.
[46] Z. Xu, J. Zhu, Z. Shu, Y. Xia, R. Chen, S. Chen, Y. Wang, L. Zeng, J. Wang, Y. Cai, S. Chen, F. Huang, H.-L. Wang, *Joule* **2024**, *8*, 1790.
[47] J.-H. Baek, S. H. Kweon, H.-J. Noh, D. H. Kweon, J.-M. Seo, S. J. Lee, S. K. Kwak, J.-B. Baek, *Adv. Sci.* **2024**, 2414012, https://doi.org/10.1002/advs.202414012.
[48] J. Zhao, R. Urrego-Ortiz, N. Liao, F. Calle-Vallejo, J. Luo, *Nat. Commun.* **2024**, *15*, 6391.
[49] X. Gao, W. Chen, *Chem. Commun.* **2017**, *53*, 9733.
[50] L. Hou, Z. Li, H. Jang, M. G. Kim, J. Cho, S. Liu, X. Liu, *Angew. Chem., Int. Ed.* **2024**, *136*, 202315633.
[51] C. Li, H. Jang, M. G. Kim, L. Hou, X. Liu, J. Cho, *Appl. Catal. B-Environ.* **2022**, *307*, 121204.
[52] Y. Wu, W. Wei, R. Yu, L. Xia, X. Hong, J. Zhu, J. Li, L. Lv, W. Chen, Y. Zhao, L. Zhou, L. Mai, *Adv. Funct. Mater.* **2022**, *32*, 2110910.
[53] C. Li, H. Jang, S. Liu, M. G. Kim, L. Hou, X. Liu, J. Cho, *Adv. Energy Mater.* **2022**, *12*, 2200029.
[54] S. Chandrasekaran, N. Li, Y. Zhuang, L. Sui, Z. Xiao, D. Fan, V. Aravindan, C. Bowen, H. Lu, Y. Liu, *Chem. Eng. J.* **2022**, *431*, 134073.
[55] L. Xie, L. Wang, X. Liu, J. Chen, X. Wen, W. Zhao, S. Liu, Q. Zhao, *Nat. Commun.* **2024**, *15*, 5702.
[56] X. Huang, R. Lu, Y. Cen, D. Wang, S. Jin, W. Chen, I. Geoffrey, N. Waterhouse, Z. Wang, S. Tian, X. Sun, *Nano Res.* **2023**, *16*, 9073.

[57] Y. Cong, L. Chen, M. Liu, H. Wang, L. Zhang, Q. Zhao, C. Li, *Chem. Eng. J.* **2024**, *495*, 153433.
[58] P. Su, W. Pei, X. Wang, Y. Ma, Q. Jiang, J. Liang, S. Zhou, J. Zhao, J. Liu, G. Q. (Max) Lu, *Angew. Chem., Int. Ed.* **2021**, *60*, 16044.
[59] R. Ding, L. Lin, C. Pei, X. Yu, Q. Sun, H. S. Park, *Chem. A., Eur. J.* **2021**, *27*, 11150.
[60] M. D. Hossain, Z. Liu, M. Zhuang, X. Yan, G.-L. Xu, C. A. Gadre, A. Tyagi, I. H. Abidi, C.-J. Sun, H. Wong, A. Guda, Y. Hao, X. Pan, K. Amine, Z. Luo, *Adv. Energy Mater.* **2019**, *9*, 1803689.
[61] T. C. Jeyakumar, C. Sivasankar, *New J. Chem.* **2019**, *43*, 1440.
[62] W. Zhang, Y. Xiao, *Energy Fuels* **2020**, *34*, 2425.